Acta Cryst. (1966). **20**, 49

The General Form of Non-Circular Diffraction Rings

BY WARTAN A. JEMIAN

Auburn University, Auburn, Alabama, U.S.A.

(*Received* 10 *October* 1964 *and in revised form* 13 *April* 1965)

A sample of polycrystalline sheet produced non-circular X-ray diffraction rings due to its preferred orientation. A general analysis was made, showing that the rings are of two types, which are caused by white and characteristic radiation. Those formed by white radiation are projections of the reciprocal lattice. A chart is given showing the various forms in which the diffracted rays lie for individual kinds of reflecting plane, as a function of the inclinations of the plane and the incident beam with the texture axis. The rings caused by characteristic radiation are composed of groups of apparently connected Debye arcs. Their connection is enhanced by large unit-cell size and scatter of crystallite orientations about the orientation of the ideal texture. This analysis is applied to the interpretation of patterns from hot-pressed pyrolytic graphite and is further demonstrated by rotating a single crystal of mica in the path of the X-ray beam.

Introduction

X-ray diffraction photographs of a thin sheet of polycrystalline graphite (Figs. 1 and 6) show eccentric rings of both circular and non-circular shapes, rather than only the expected circular Debye rings. A study was made to determine the origins of these shapes. Their analysis and description are presented in a general way since they arise in other studies. The rings will be circular and concentric only when the sample is specially aligned with the incident beam (Fig. 2). Leonhardt (1924) analyzed patterns showing asterism from bent crystals, which correspond to some of the non-circular rings found here. They are equivalent in form to the rotating mirror light reflections described by Schwarzmann (1900, 1901). However, neither of these analyses nor others of a similar kind that are reviewed in *Internationale Tabellen zur Bestimmung von Kristallstrukturen* (1935) show the details and extent of the possible individual figures. The remaining non-circular rings originate in a different manner.

The graphite is similar to that described by Ubbelohde, Young & Moore (1963). It was prepared by pressing pyrolytic graphite at a temperature close to 3000°K (Carter, 1964), which tended to align the basal planes of the hexagonal crystallites normal to the direction of compression without restricting the alignment in other directions. This forms a compression texture which is a type of fiber texture which may also be generated by rotating a single crystal about a fixed axis and randomly assigning orientations from this set to the crystallites. In this sample the texture axis is normal to the surface of the sheet. The similarity is demonstrated by rotating a mica crystal in the path of the incident beam.

All X-ray patterns were made with flat film cameras with the film normal to the incident beam. Unfiltered

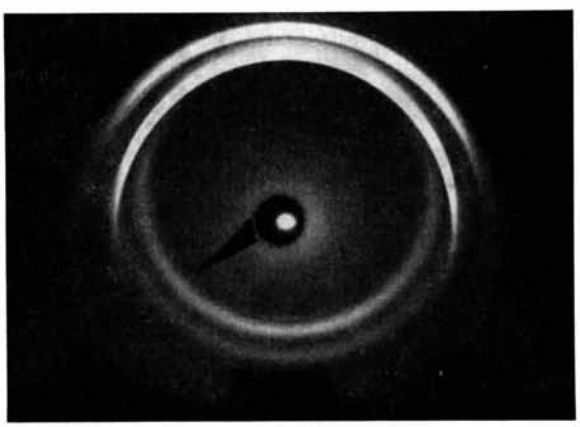

Fig. 1. Transmission pattern of hot-pressed pyrolytic graphite. Tilt angle is 4·1°, downwards.

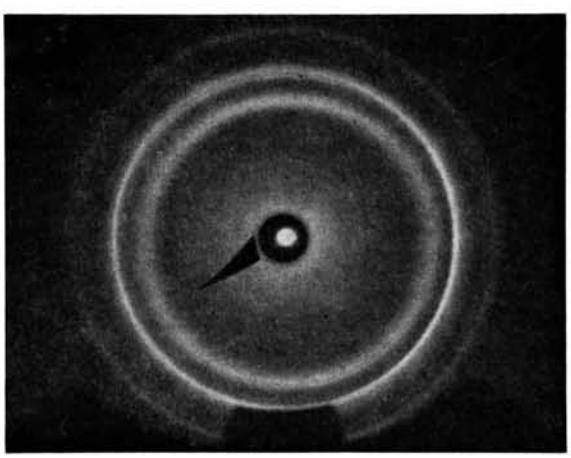

Fig. 2. Transmission pattern of general figures at 0° tilt.

copper radiation, collimated by a pinhole tube, was used. Filtering the radiation in the usual way only eliminates portions of the patterns but allows their outlines to remain. Other conditions were tried to test specific aspects, but they do not provide additional information.

Analysis

The diffraction figures of samples with fiber texture are of two types. White radiation produces 'general figures', and characteristic radiation produces 'characteristic figures' and contributes to the general figures. These are analyzed separately.

The Bragg diffraction condition, the spectral variation of intensity, and the film geometry affect the appearance of the patterns in detail but do not alter the forms. Therefore, these factors will not be discussed. Also, it is assumed that the stereographic projection and Ewald construction for the diffraction condition are sufficiently well-known that reference may be made to them without accompanying figures.

General figures

The reciprocal lattice of the polycrystal with fiber texture consists of circular rings concentric with the texture axis. Each of these corresponds to reciprocal lattice points of equivalent planes in a single crystal. If some of the crystallites are not aligned exactly according to the ideal texture, the rings will take on the form of annular rings on the surface of a sphere centered at the origin of the reciprocal lattice. A reciprocal lattice vector from the origin to a point on one of these rings defines a pole to a plane in one of the real crystals. Thus the reciprocal lattice rings represent cones-of-poles of planes in the sample.

The incident X-ray beam may be considered to be reflected, as a result of diffraction, across each pole by equal angles just as the equal angles of incidence and reflection criterion is applied to a diffracting plane. This is illustrated in Fig. 3 with the incident beam directed along OC and the crystal at C. AC is the texture axis. After the incident beam is reflected across a pole such as CP, a corresponding reflected ray, CR, is produced. The reflected rays form a conical figure called the reflected cone.

The shapes of the reflected cones may be developed using the stereographic projection as demonstrated in Fig. 4. The direction of the incident beam is taken at the center of the map so that all projections may be made along radial lines. The map bisects the reference sphere so that all figures are projected onto it from the appropriate pole of the primitive circle (Sohon, 1941). Both the primitive circle (marked 90°) and the 45° circle are drawn in heavy lines. The circle-of-poles, which is the projection of the cone-of-poles, is shown as a dashed line. The points of this circle lying within the 45° ring produce back reflections, and the points lying between the 45° and primitive circles produce diffracted rays in transmission.

The parameters, apex angle and tilt angle, specify the ring form. Fig. 5 represents all possible combinations and shows a number of the diffraction figures. In each of these the transmission portion is shown solid, the back reflection portion is dashed, and the tilt direction is taken upwards, so that the projection of each texture axis falls at a point above the center of the corresponding stereogram.

The field of Fig. 5 may be subdivided into regions according to the values of the parameters, σ = Tilt Angle + Semi-Apex Angle and δ = Tilt Angle − Semi-Apex Angle. The chart also shows the regions where the patterns are either in back reflection, transmission, or are mixed, the conditions under which one or two leaves will be formed, size trends, and other details.

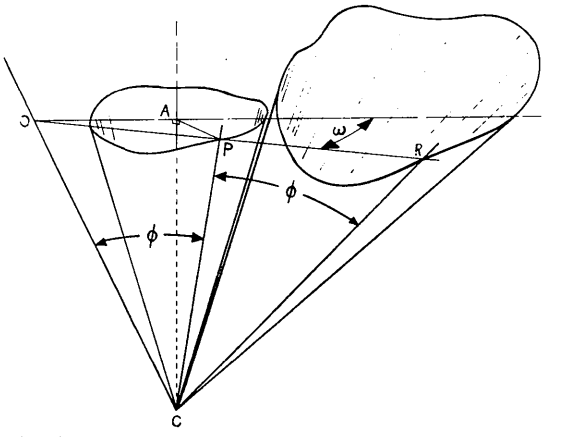

Fig. 3. The geometry of the incident beam, cone-of-poles, and reflected cone.

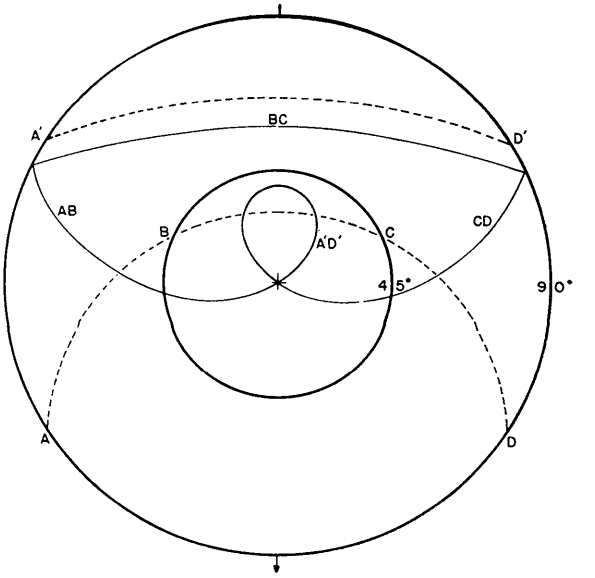

Fig. 4. Stereographic projection of circle-of-poles (dashed) and reflected rings (solid) for a cone-of-poles of 140° apex angle and 40° tilt. The direction of tilt is downward.

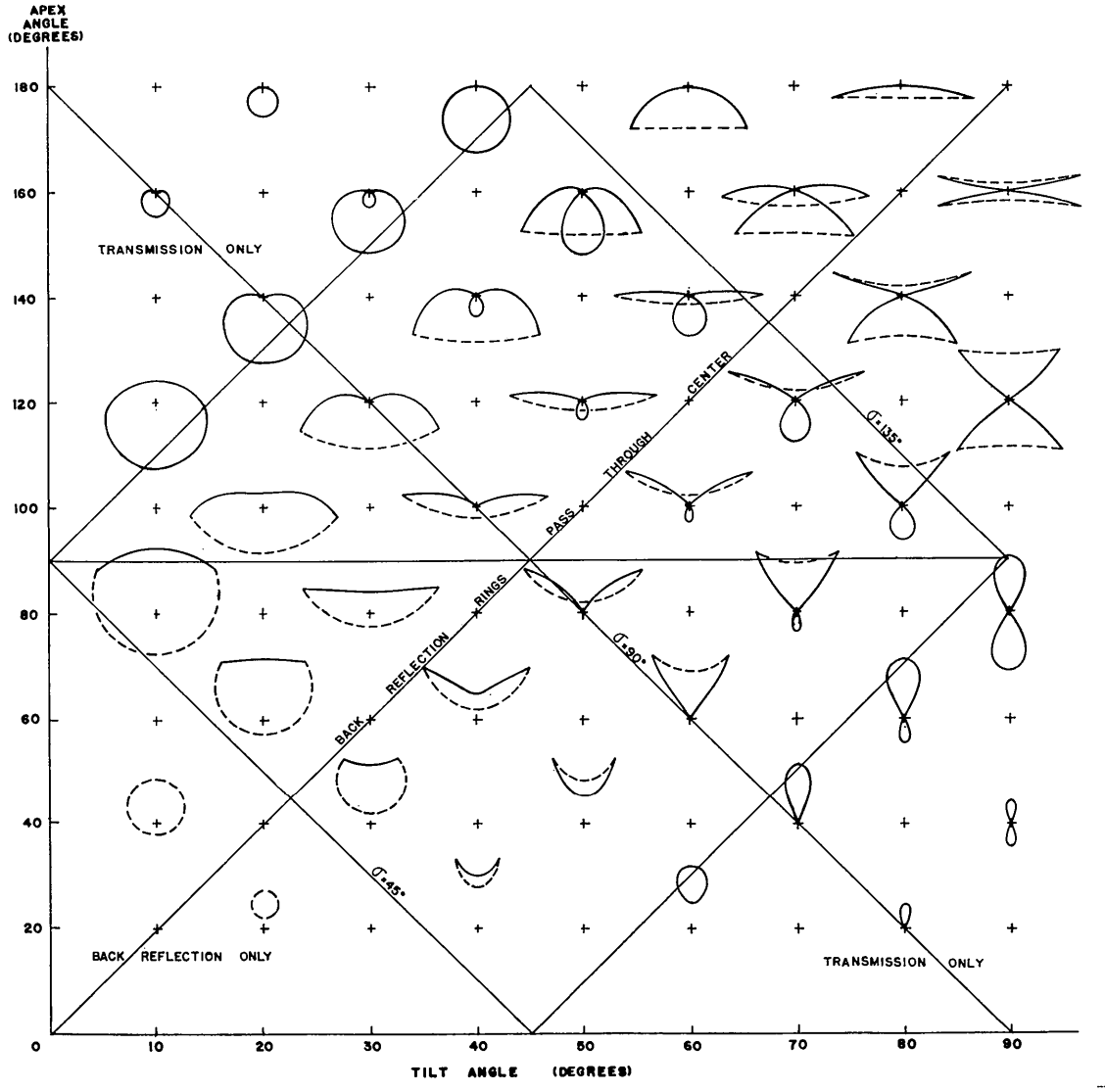

Fig. 5. Chart of reflected figures in stereographic projection as a function of apex angle of the cone-of-poles and tilt angle. Transmission figures are shown solid and back reflection figures are dashed. The direction of tilt is taken vertically upward in each stereographic figure.

The appearance of a ring, with respect to shape and curvature, may be misleading. In the case of back reflection patterns, the rings are only approximately round. There are no conic figures possible except when the tilt angle is 0° or when the apex angle is 180°. This is illustrated by the following analysis.

Referring to Fig. 3, construct a plane, $OAPR$, that is normal to the axis of the cone-of-poles, AC. Set up a polar coordinate system with origin at O as shown. The cone-of-poles intersects $OAPR$ in a circle

$$\varrho^2 = r^2 + 2a\varrho\cos\omega - a^2 \qquad (1)$$

where r is AP, a is OA, and ϱ is the polar distance of P. Both r and a are trigonometric functions of the apex and tilt angles, respectively. The polar distance of R is ϱ' and is related to ϱ (Burton, 1964):

$$\varrho' = \varrho\left(1 + \frac{D^2}{K^2 - \varrho^2}\right). \qquad (2)$$

K and D are OC and PC, respectively, and are functions of r, a, and the distance AC, which is arbitrary. Combination of (1) and (2) yields curves of powers too high to be conics except when $a = O$ or apex angle $= 180°$. This complexity also excludes the possibility that figures such as those formed by 20° tilt-140° apex and 30° tilt-160° apex may be cardioids and limacons, although the resemblance is strong.

The general form of the back reflection patterns is either single-leaved closed loops or arcs across the tilt direction. The transmission figures include single- and double-leaved closed rings and various forms of arcs. When σ is equal to or greater than 90°, the reflection

cone has a sharp edge or crosses itself. The resulting reflection figures form a sharp point at the center with zero radius of curvature or cross.

A feature requiring special clarification is the shape of the portion of the reflected ring that is close to the center of the map when the value of σ is very close to but less than 90°. When $\sigma=90°$, a sharp apex is formed in the reflecting ring; but the apex has a finite radius of curvature for other values of σ, however close. These portions of the curve will always lie along the line of symmetry on the map or film, and their slope may be determined by differentiating (2) with respect to ω.

$$\frac{d\varrho'}{d\omega} = \left[1 + \frac{D^2}{K^2-\varrho^2} + \frac{2D^2\varrho^2}{(K^2-\varrho^2)^2}\right]\frac{d\varrho}{d\omega}. \quad (3)$$

Therefore, the slope of the reflected ring, $d\varrho'/d\omega$, will be zero whenever the slope of the circle-of-poles, $d\varrho/d\omega$, is zero.

In some of the figures where σ is close to but less than 90°, the curvature of the transmission figures changes sign. For example, consider any fixed apex angle. Increase the tilt angle so that σ approaches 90°, and the figure will tend to become either heart-shaped or tear drop-shaped if the apex angle is either greater or less than 90°, respectively. In the former case one inflection point will occur in each branch of the ring, and in the second case two will develop. These inflections are related to the distortion of the map or flat film, both of which involve tangent functions, increasing as σ approaches 90°.

The reflection conditions and distortion by projection have competing effects on the slope, $d\varrho'/d\omega$, of the reflected figure. The first of these is described by (3), and the second increases with radial distance on the plane. Regardless of the presence of inflections, the reflection ring becomes narrower from the broadest part of the ring toward the center of the map or film. These inflections are not a part of the reflected cone.

Characteristic figures

The possible reciprocal lattice rings lie in reciprocal lattice layer planes and along cylinders and cones concentric with the rotation axis.

Referring to the Ewald construction, the sphere of reflection will be intersected at points along circular rings by the layer planes. These account for reflected beams along surfaces of right circular cones and will strike the flat film at points along ellipses, parabolas, and hyperbolas.

Characteristic figures may be accounted for by sets of reciprocal lattice rings that define cylinders or cones, that are concentric with the rotation axis. The nature of the connection depends on the particular orientation relationships involved. In general, the figures are not simple because the line of intersection between a sphere and a right circular cylinder or cone is not a conic, but is generally complex in form.

Other examples

The cones of diffracted rays will be right circular when the apex angle is 180°. However, all of the figures pass through the center of the map and cannot be circular on the film. The traces will be conics as in the cases of loci of zonal spots in Laue single crystal patterns.

When the tilt angle is 90°, the diffracted cones and the pattern will be symmetrical across the equator of the map. Cullity (1959) shows an example of this.

Buerger & Dollase (1964) show figures that are analogous to those described here for apex angles of 160° at several tilt angles between 0° and 20°. In this case the figures mark the boundaries of the recorded areas in precession photographs, but the geometry is the same.

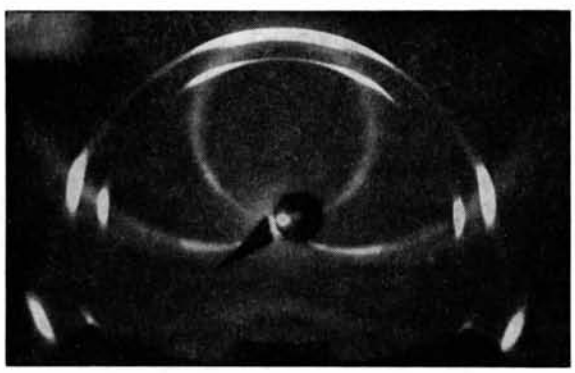

Fig. 6. Transmission pattern of graphite at 14·8° downward tilt.

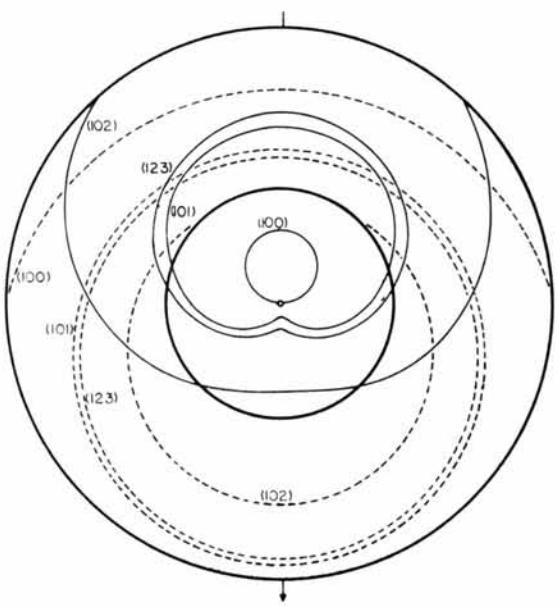

Fig. 7. Stereographic projection of cones-of-poles and reflected cones, for transmission only, for {100}, {101}, {123}, and {102} planes of graphite at a tilt angle of 14·8° downward.

If the fiber texture is sharp, the characteristic figures will be composed of lines of discrete spots; but if the texture is not sharp, there may be an appreciable amount of connection between the spots. Each spot is a short Debye arc from a different set of planes and can be indexed by standard methods. The number of planes that may contribute reflections within a given angle from the incident beam increases with increasing size of the unit cell.

Applications and examples

Hot-pressed pyrolytic graphite

The texture axis of the graphite is [001]. Figs. 1 and 6 contain both characteristic and general figures. In Fig. 1 both characteristic figures are due to reflections from {101}. The outer curve is due to $K\alpha$ and the inner due to $K\beta$. The inner general figure is {101} and the outer is {123}. In Fig. 2 the rings are indexed as {101}, {123}, and {034} general figures from the inside towards the outside. A greater number of planes may be identified if desired, and a greater number of rings of general figures become visible with longer exposure of the film. The general figures in Fig. 6 are identified as {100}, {101}, {123}, and {102}. Fig. 7 is a stereographic construction of the transmission portion.

Fig. 8. Transmission pattern of mica rotated about the pole to its basal plane at a tilt angle of 16°, downward.

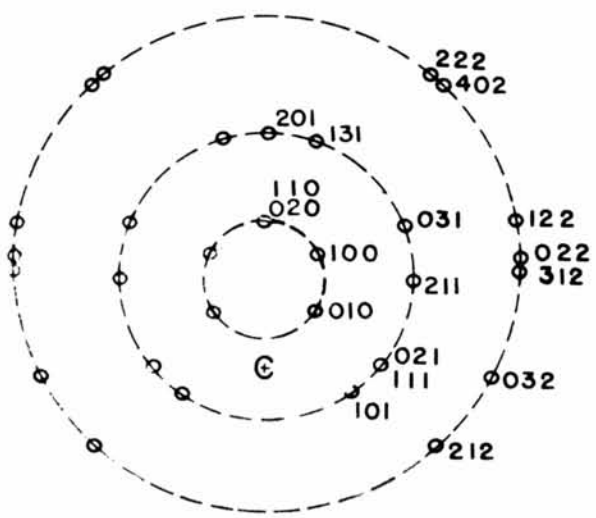

Fig. 9. Stereographic projection of poles of some reflecting planes for the $l=0$, $l=1$, and $l=2$ reciprocal lattice layers of mica.

The spots in the characteristic figures of Fig. 6 are due to {100}, {101}, and {102}. The {123} does not contribute. This selection is consistent with the intersection of the reflection sphere by a cylinder of rings.

Synthetic fiber texture

Fig. 8 is a transmission pattern of mica with synthetic fiber texture. The multiplicity of figures makes specific indexing uncertain; however, the forms substantiate the analysis. The characteristic figures are elliptical. The $l=0$ layer is barely visible, the $l=1$ layer and $l=2$ layer rings are quite complete in both $K\alpha$ and $K\beta$, and only light traces of the $l=3$ layer ring may be found. Fig. 9 is a stereographic plot of some of the reflections that contribute to those rings. At the 16° tilt angle the $l=13$ layer ring will be the lowest layer to produce a hyperbolic characteristic figure. A parabolic characteristic figure may be formed by the $l=0$ layer at a 45° tilt angle, which is a general condition for any crystal.

Summary and conclusions

When the crystallites are randomly oriented in a sample the reciprocal lattice points will not be grouped into special forms, and the characteristic radiation, because of its relative intensity, will produce Debye rings on the film. In the case of preferred orientation, the lengths of the Debye rings will be limited because only chance alignments will satisfy the Bragg condition. In some textured samples the conditions may allow the formation of apparently continuous, non-circular rings due to characteristic radiation from a sequence of different crystallographic planes. This tendency will be greater with larger unit-cell sizes and with increasing scatter of the alignment of crystallites about the orientation of the ideal texture.

Any condition of preferred orientation or distortion, although limited, as in bending, will allow the formation of circular rings or arcs in the reciprocal lattice, which will be projected as non-circular rings or arcs on a piece of flat film. The circular reciprocal lattice rings or arcs correspond to the individual reciprocal lattice points of a single crystal of the material. Fig. 5 can be used to analyze them individually.

The author gratefully acknowledges the assistance of Dr L. P. Burton, Professor of Mathematics, and several students at Auburn University. J. W. O. Anderson and J. N. Knight aided in the indexing of the patterns, and J. A. Botts prepared the line drawings with

enthusiasm. Graphite samples were kindly furnished by M. B. Carter, Advanced Materials Laboratory, Union Carbide Corporation, Lawrenceburg, Tennessee. The study was supported by the Engineering Experiment Station of the School of Engineering, Auburn University.

References

BUERGER, M. J. & DOLLASE, W. A. (1964). *Science*, **145**, 264.
BURTON, L. P. (1964). Private communication.
CARTER, M. B. (1964). Private communication.
CULLITY, B. D. (1959). *Elements of X-ray Diffraction*, 93.
Internationale Tabellen zur Bestimmung von Kristallstrukturen (1935). Vol. II. Berlin: Bornträger.
LEONHARDT, J. (1924). *Z. Kristallogr.* **61**, 100.
SCHWARZMANN, M. (1900). *Neues Jb. Miner.*, **2**, 1.
SCHWARZMANN, M. (1901). *Neues Jb. Miner.*, **1**, 9.
SOHON, F. W. (1941). *The Stereographic Projection.*
UBBELOHDE, A. R., YOUNG, D. A. & MOORE, A. W. (1963). *Nature, Lond.* **198**, 1192.

Acta Cryst. (1966). **20**, 54

The Crystal Structure of 1,4-Piperazine-γ,γ-dibutyric Acid

BY R. POTTER

Viriamu Jones Laboratory, University College, Cardiff, Wales

(*Received* 13 *May* 1964 *and in revised form* 20 *May* 1965)

1,4-Piperazine-γ,γ′-dibutyric acid crystallizes in the space group $P2_1/a$ with two molecules of

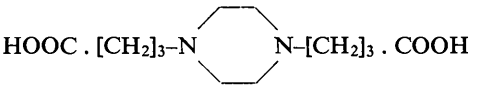

in the unit cell of dimensions $a = 15{\cdot}554 \pm 0{\cdot}004$, $b = 6{\cdot}502 \pm 0{\cdot}002$, $c = 6{\cdot}702 \pm 0{\cdot}002$ Å; $\beta = 91{\cdot}54° \pm 0{\cdot}04°$.

A trial structure was obtained by a sign-relation method developed for three dimensions, and this has been refined by electron-density and least-squares syntheses. The only hydrogen bonds in the structure are between hydroxyl oxygen atoms and the ring nitrogen atoms in adjacent molecules; the O —— H · · · N distance is $2{\cdot}60 \pm 0{\cdot}01$ Å.

Introduction

1,4-Piperazine-γ,γ′-dibutyric acid,

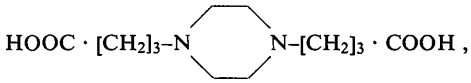

was prepared during investigations in polymer chemistry. The infrared spectrum does not correspond with either the dimer form

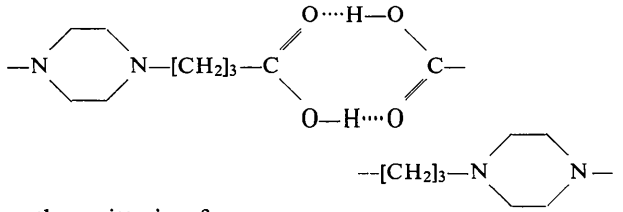

or the zwitterion form

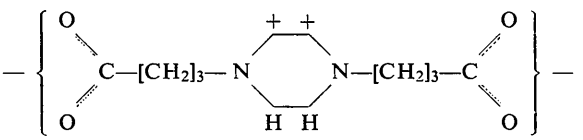

of hydrogen bonding, although the potassium salt and the hydrochloride give the expected spectra (Stace, 1962). It appeared therefore that the hydrogen bonding should be investigated by X-ray analysis. [A preliminary report of the structure has already been published (Potter, 1962)].

Experimental

This amino acid crystallizes from anhydrous methanol in the presence of dry ether as colourless laths which cleave very readily parallel to (100). Care was necessary during all operations to keep moisture out, as the substance has a great affinity for water. The crystals last only a few hours on exposure to air; they gradually turn white owing to uptake of water. When the crystals are coated with a clear thixotropic varnish, their crystalline 'life' is increased to a few days.

Oscillation and Weissenberg photographs taken with Cu $K\alpha$ radiation indicated the Laue symmetry $2/m$, with systematic absences $h0l$ for h odd and $0k0$ for k odd, thus uniquely determining the space group as $P2_1/a$. The unit cell dimensions are:

$$a = 15.554 \pm 0.004,\ b = 6.502 \pm 0.002,\ c = 6.702 \pm 0.002 \text{ Å}$$
$$\beta = 91.54° \pm 0.04° .$$

$D_m = 1.27$ g.cm^{-3}; $D_x = 1.24$ g.cm^{-3}; $Z = 2$.

Absorption coefficient for Cu $K\alpha$ radiation, 9 cm^{-1}.